Crystalline As_2Se_3: Electronic and geometric structure

Eugen Tarnow, A. Antonelli, and J. D. Joannopoulos
Department of Physics, Massachusetts Institute of Technology, Cambridge, Massachusetts 02139
(Received 13 March 1986)

Realistic *ab initio* total-energy calculations are performed to investigate the electronic and geometric structure of crystalline As_2Se_3. Results include the following: total energies for various distortions, the equilibrium geometric structure, intralayer and interlayer cohesive energies, charge densities, the density of states, the band structure, rigid-layer phonon frequencies, and effective masses. Specific attention is focused on studying the nature of bonding within and between layers, as well as elucidating the nature of the electron and hole wave functions in the vicinity of the fundamental gap. In particular it is found that the interactions between the layers are crucial in determining the properties of the wave functions at the band edges. Moreover, the electron and hole masses are predicted to exhibit a large and unusual anisotropy.

I. INTRODUCTION

For many years now, considerable attention has been directed towards understanding the electronic, optical and magnetic properties of the arsenic chalcogenides and other V-VI compounds.[1,2] Unfortunately, comparatively little firm theoretical knowledge exists concerning the nature of their ground states and excited states. In their crystalline form these materials are quite complex with large unit cells typically containing 20 atoms. This complexity has made realistic, parameter-free theoretical calculations very difficult. For example, theoretical information on As_2Se_3 has been limited, to our knowledge, to simple empirical[3–5] and semiempirical[6] calculations of electronic states. Clearly it is of great importance to have a good understanding of the electronic and total-energy structure of such crystals before we can hope to reach any meaningful conclusions regarding the local bonding configurations in the glasses, the nature of intrinsic defects in the materials and the sources of the negative effective correlation energy.

In this paper we present the results of the first realistic *ab initio* pseudopotential calculation of the electronic and geometric structure of crystalline As_2Se_3. The only inputs into the calculation are the atomic numbers of the constituent atoms. Many interesting results emerge, including the accuracy with which the structural parameters can be "predicted," the different energy scales associated with various types of structural distortions, the nature of the electronic charge density of the system, the nature of the intralayer (within a layer) and interlayer (between layers) bonding, the characteristics of the electronic charge distribution in the vicinity of the band edges, the locations of the smallest direct and indirect gaps in the Brillouin zone, and the unusual properties of the electron and hole effective masses.

The format of this paper is as follows. We begin in Sec. II with a brief description of the crystal structure. In Sec. III we describe the details of our calculational procedure, its foundation, reliability and accuracy. In Sec. IV we present all the results. These include the total energies for various structural distortions, total charge densities in several regions of the crystal, and a band structure and density-of-states calculation. We also examine the nature of the charge distribution in various bands and gap-edge states, identify the extrema of the band edges, and calculate the corresponding electron and hole masses. This is followed by a calculation of the cohesive energy and bonding energies associated with the intralayer and interlayer interactions, and a construction of a simple tight-binding Hamiltonian based on the calculated realistic band structure. Finally in Sec. V we give a summary and some concluding remarks.

II. STRUCTURE

As_2Se_3 exists in a monoclinic (very nearly orthorhombic) crystal structure with atoms arranged in layers.[7–9] There are 2 layers and 20 atoms in a unit cell. A cross section through the layers is shown schematically in Fig. 1. The As atoms exist in two distinct types of environments [As(1) and As(2) in our notation] with each As atom bonded to three Se atoms. The Se atoms exist in three types of environments [Se(1), Se(2), and Se(3)] with each Se bonded to two As atoms. As and Se atoms of type 1 and 2 form chains that spiral around axes perpendicular to the plane of the figure. The chains are interconnected by Se atoms of type 3.

The symmetry operations of the crystal are a mirror plane perpendicular to the b axis with an associated translation, inversion, their products, and the identity. The layers in the unit cell are related to each other by a rotation of π about the b axis.

We note that each layer, when projected onto the a-b plane, forms a sawtooth pattern. The stacking of layers evidently involves the fitting of one pattern onto another. Interestingly, this fitting could also be accomplished without having to rotate alternate layers around the b axis. The reason, however, that this alternation is preferred, is more subtle. Although it is not clear to us what the precise mechanism is we speculate the following. A reasonable assumption is that the most important interactions are due to the outermost [As(1)-Se(1)] and [As(2)-

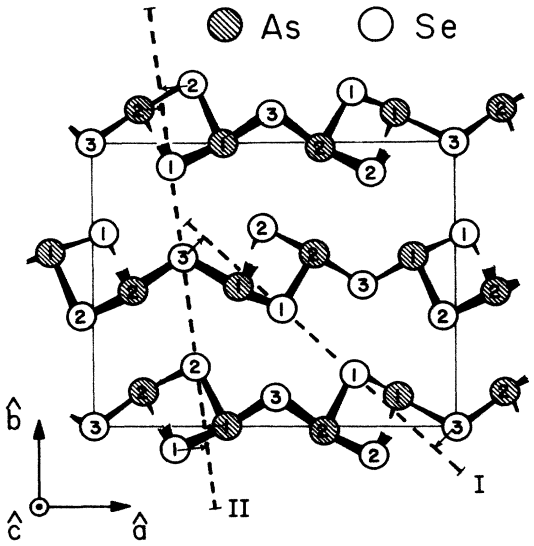

FIG. 1. Three-dimensional schematic illustration of the structure of As_2Se_3 showing portions of three layers. The layers lie perpendicular to the plane of the figure. The unit cell contains 20 atoms divided between 2 layers. Within a layer As and Se atoms of types 1 and 2 form spiraling chains running perpendicular to the figure. Neighboring chains are linked together by Se atoms of type 3. Dashed lines represent cross sections through planes lying perpendicular to the figure. These planes are useful for examining the charge densities.

Se(2)] pairs of adjacent layers. Modeling these as rigid rods we find, simply, that neighboring layers are more easily close packed if they are rotated by π.

The initial coordinates of the atoms in the unit cell (which were found to be adequate for a self-consistent treatment throughout) were taken from Vaipolin.[7] The unit cell was chosen to have an orthorhombic shape with the experimental lattice constants $a=12.05$ Å, $b=9.89$ Å, and $c=4.28$ Å. The deviation from the monoclinic unit cell is extremely small and amounts to a 0.5° tilt in the b axis off the normal to the a-c plane. As remarked before,[5] this simplifying change does not introduce any extra symmetries and, due to its minuteness, is insignificant in effect.

III. METHOD OF CALCULATION

The calculations were performed within the framework of density functional theory using the local-density approximation, and the pseudopotential approximation.[10] Further approximations involved truncations in the number of basis states used, and selected summation over states in the Brillouin zone. For completeness we begin with a review of each of these concepts.

Very briefly, density functional theory allows one to map the many-body problem of an interacting electron gas in an external potential onto that of a system of noninteracting particles moving in some effective single-particle potential. This mapping is exact in principle. Unfortunately, we do not know precisely what this effective potential is. Nevertheless, sufficiently good approximations to it exist, that this approach works extremely well.[10] For our calculation we have chosen the Wigner interpolation scheme,[11] although other schemes give very similar results.

TABLE I. Convergence of the cohesive energy with respect to the number of special **k** points used.

	Number of **k** points		
	1	8	27
E_{coh} (eV)	2.5	3.1	3.1

The strong electron-nucleus interaction can be handled within the framework of pseudopotential theory. In this approximation one replaces the true electron-nucleus potential by a much weaker effective potential—a pseudopotential. This has many of the scattering properties of the original potential but allows one to model only the valence electrons of the system. Since it is the valence electrons that are responsible for nearly all the physical and chemical properties of the solid this scheme is very versatile.[10] We have used the procedure proposed by Hamann, Schlüter, and Chiang[12] in order to generate our pseudopotentials. Typically one expects the pseudocharge density and all-electron charge density to be the same outside the core region of each atom, which is roughly 0.5 Å in radius.

Calculations of the electronic charge density, in principle, involve a summation over each **k** point in the Brillouin zone. This can be significantly simplified by using the special-**k**-point scheme.[13] Here one can obtain a good average with only a few, carefully selected points. A check of convergence with increasing sets of special **k** points is given in Table I. We note that the cohesive energy converges rapidly to within 0.1 eV. The individual Fourier components of the potential changed by 10% going from 1 to 8 **k** points and by less than 1% going from 8 to 27 **k** points. The sums over the Brillouin zone were generally done using the special **k** point (0.25,0.25,0.25) (Ref. 14) and its seven permutations.

Since the ionic pseudopotentials and screening potentials are weak they can be conveniently expanded in terms of plane waves. We use two sets of plane waves: The first set is included in diagonalization (including plane waves with kinetic energies less than E_1) and the second set is included in second-order perturbation theory[15] (kinetic energies less than E_2). Tests of several calculational results are given in Table II. These include convergence of the cohesive energy, convergence of total-energy differences for intralayer and interlayer distortions, convergence of the difference in energy of the highest valence band at (0.25,0.25,0.25) and (−0.25,0.25,0.25), and finally convergence of a direct transition energy at (0.25,0.25,0.25). We note that our results are converged to about 0.2 eV per atom in the cohesive energy, and 0.01 eV in the total-energy differences. The energies of the filled bands and gaps are converged to better than 0.05 eV. In our calculations we chose to use the cutoffs to be $E_1=5$–6 Ry and $E_2=10$–12 Ry.

In order to speed up the convergence of the self-

TABLE II. Convergence of several calculational results with respect to the size of plane-wave basis used. E_{coh} is the cohesive energy; Δ_1 is the total energy for an intralayer distortion (uniformly decreasing the nearest-neighbor bond length by 10%); Δ_2 is the total-energy difference for an interlayer distortion (decreasing the layer spacing by 15%); ε_1 is the direct transition energy at $(\frac{1}{4},\frac{1}{4},\frac{1}{4})$; ε_2 is an eigenvalue difference for different **k** points [the energy of the top of the valence band at $(\frac{1}{4},\frac{1}{4},\frac{1}{4})$ and $(-\frac{1}{4},\frac{1}{4},\frac{1}{4})$]. The cutoffs are indicated in terms of the kinetic energy and the corresponding number of plane waves. E_1 labels the basis set used in diagonalization, and E_2 refers to the basis set included in second-order perturbation theory (Ref. 15). E_1 and E_2 are expressed in Ry.

	$E_1=4$, $E_2=8$ 460,1300	$E_1=5$, $E_2=10$ 650,1850	$E_1=6$, $E_2=12$ 850,2400
E_{coh} (eV)	2.5	3.1	3.3
Δ_1 (eV)	0.00	0.56	0.56
Δ_2 (eV)	0.056	0.075	0.071
ε_1 (eV)	1.56	1.57	1.53
ε_2 (eV)	0.24	0.21	0.21

consistent procedure a dielectric matrix method[16] was used for the lowest 113 Fourier components of the potential. In a typical run six iterations were required to obtain consistency in the total energy to within 1 meV. It was not possible to go beyond this accuracy due to the presence of computational noise.

Systematic errors are more difficult to estimate but one finds, typically, that lattice constants can be "predicted" to within a few percent, phonon frequencies to within 10%, and even cohesive energies to within 20%.[10] In fact the accuracy in the cohesive energy is very good considering that it involves a difference in energy between substantially different systems, i.e., isolated atoms and the bulk solid.

Using a converged potential the band structure was calculated along lines in the irreducible portion of the Brillouin zone. The eigenvalues at 80 points along the chosen lines were calculated and a smooth interpolation was made to connect these. These data, complemented with a calculation of the eigenvalues at 108 evenly spaced **k** points in the irreducible Brillouin zone, was the basis for determining the extrema of the band edges.

IV. RESULTS

A. Total charge densities

The total electronic charge density can provide interesting information concerning the nature of bonding both within and between the layers of the material. To display the charge density one needs to find suitable planes to cut through the crystal. Due to the complexity of the unit cell, however, there are many different possible planes to choose. We have examined several of these and find three planes that are most informative.

Planes I and II are sketched in Fig. 1. They both run perpendicular to the plane of the figure. Plane I passes through Se(1) atoms of adjacent layers with some projected electronic density from As(1) and Se(3) atoms. Plane II includes all the three types of Se atoms, each of them in a different layer, with further As(1), As(2), Se(1), and Se(2) atoms slightly above and below the plane. The third plane, plane III (not shown in the figure) passes through three atoms of a single layer—Se(3), As(1), and As(2).

In Fig. 2 we show the total charge density through the different planes. In plane I, Fig. 2(a), we find the following salient features. The charge distribution is very covalent and one can identify bond charge between the As and Se atoms. We note in addition a considerable charge overlap between adjacent layers. Such large overlap is not observed, for example, between chains (the corresponding molecular structures) in trigonal Se.[17,18] Moreover, the overlap in As_2Se_3 is not an effect of the lone-pair states projecting out into the interlayer region as one might naively expect. Rather we have found that it is a consequence of overlap between the back lobes of the *p*-like bonding states in neighboring layers. This appears to be purely a geometric property of the stacking of layers. Finally, we also note that there is non-negligible charge overlap between third nearest-neighbor Se(1) and As(1) atoms in the same layer and within a chain.

Figure 2(b) shows the total charge density in plane II. Here the overlap between layers is much smaller than in plane I. We note that the charge overlap between third nearest-neighbor Se(1) and As(1) atoms within the chains can again be observed in the bottom layer of the figure.

In Fig. 2(c) we show the total charge density in plane III. Here we notice that there is a very small asymmetry that distinguishes between the As(1) and As(2) atoms. The As(1)-As(2) asymmetry most likely arises from secondary interactions between the layers. In fact, as we shall discuss in Sec. IV B, the energy associated with this asymmetry is calculated to be only about 2 meV. In this plane the bonding charge between the Se and As atoms is clearly visible. The larger bond charge between Se(3) and As(2) is associated with a shorter bond length. We also note that the interaction of the Se(3) atom with any other atoms appears to be quite small.

It is very interesting to investigate the effects of the layer-layer interactions on the intralayer bonding. This can be accomplished quite easily by simply moving the layers far apart. In Fig. 3 we present the total charge densities for As_2Se_3 with the layer separation *increased to 10* Å. At this distance, the layers essentially do not interact. The results are quite striking. The charge distributions look virtually identical to those of Fig. 2. This indicates

that the layer-layer interactions play a very minor role in determining the intralayer bonding. These interactions are important, however, in affecting the character and energies of the single-particle levels as will be discussed in Secs. IV D and IV E.

B. Total energies

To determine the structure of the material theoretically, we have calculated the total energy of the system as a function of various configurational coordinates of the

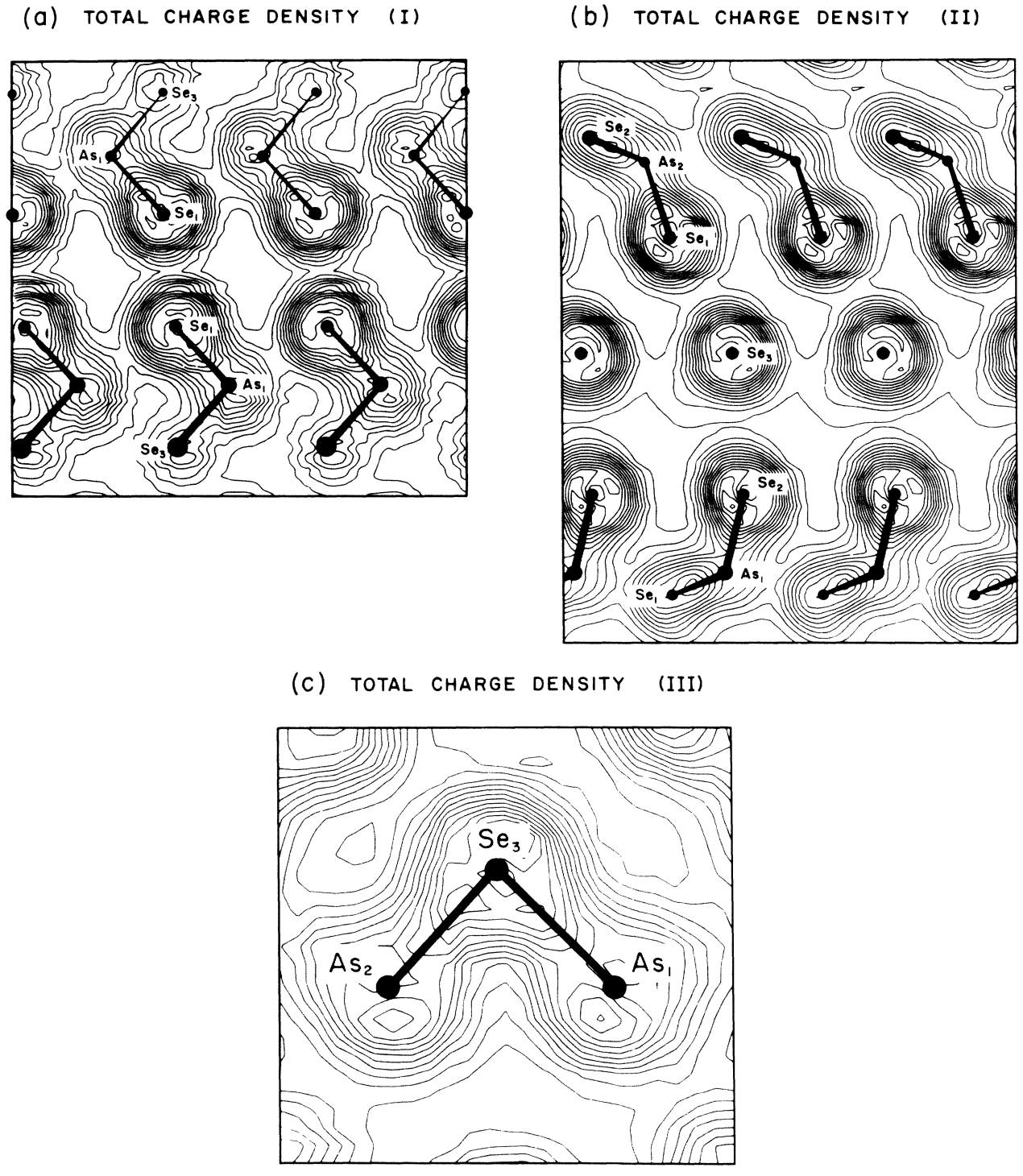

FIG. 2. Charge-density contour plots. (a) Total valence electron density in plane I of Fig. 1. Selenium atoms of type 1 lie directly in the plane. The As and Se atoms at the top and bottom of the figure lie, respectively, slightly below and slightly above this plane as indicated. (b) Total valence electron density in plane II of Fig. 1. The Se atoms of types 1, 2, and 3 near the center of the figure lie almost directly in this plane. The As and Se atoms of type 2 at the top of the figure lie, respectively, slightly above and below this plane. (c) Total valence electron density in plane III. Nearest neighbors As(1), Se(3), and As(2) lie in this plane.

atoms. Although, in principle, this would imply a complex search for a minimum in many dimensions, it is simpler and more instructive to focus on configurational coordinates that can separately distort only bond lengths within a layer, only bond angles, and only the interlayer distance and stacking position. We also investigated the effects of imposing an additional mirror symmetry within each layer. The total energies associated with the various distortions, in addition, provide information about the scale of energies for the intralayer and interlayer bonding interactions.

In Fig. 4(a) we show the total energy calculated as a

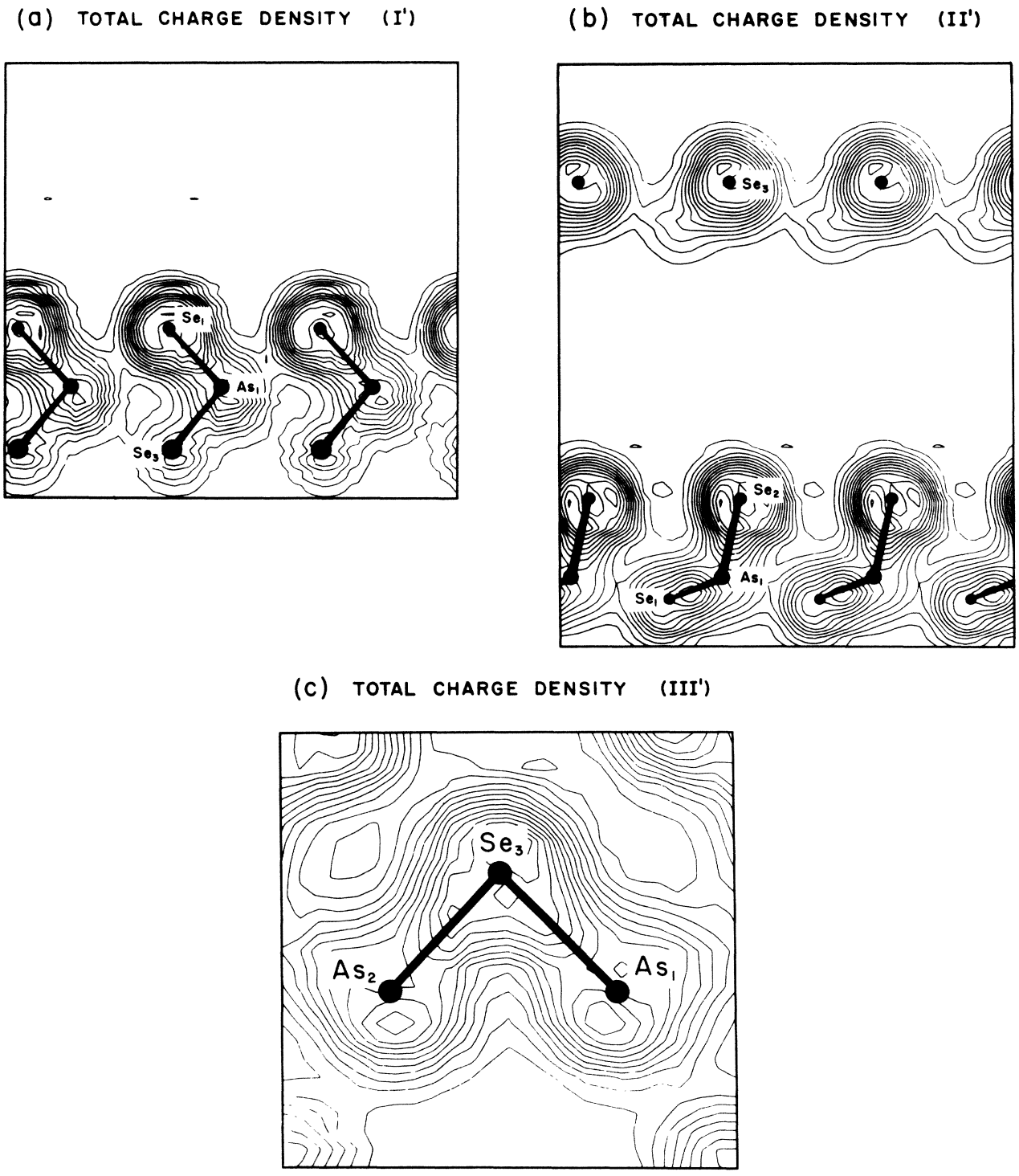

FIG. 3. Charge-density contour plots using the same conventions as in Fig. 2. The primes are used to indicate that these planes are associated with a crystal whose interlayer separation has been increased to 10 Å.

function of intralayer distortion. This distortion consists of a uniform change in the scale of bond lengths, keeping bond angles and the interlayer distance and stacking position fixed. The minimum of the calculated total energy occurs at bond lengths which are only a fraction of a percent higher than the experimental value. In Figs. 4(b) and 4(c) we examine the effects of distorting the bond angles within and between chains, keeping bond lengths and interlayer positions fixed. The results reveal that the theoretical minimum in energy occurs at bond angles whose largest deviation from experiment is only -3.5%. In Figs. 4(d) and 4(e) we consider the effect of sliding the layers rigidly along the a and c directions, respectively, keeping the interlayer distance fixed. Finally, in Fig. 4(f) we vary the distance between layers keeping everything else fixed. Again the agreement is excellent with theoretical values of interlayer stacking position and distance less than 5% from experimental measurements. These results are surprisingly good in light of the difficulties of modeling the weak intermolecular binding of a molecular crystal. Evidently, the local-density approximation is slightly overestimating the strength of this binding.

Comparing the energy scales in Figs. 4(d) and 4(e) we note that there is a large energy difference between the two shear distortions. Looking back at the crystal structure (Fig. 1) we can understand why. Sliding the layers along the a direction makes atoms of adjacent layers collide, because the "sawtooth" pattern of one layer does not fit onto the other. On the other hand, sliding the layers in the c direction produces no such interference. The softness of this shear is related to the van-der-Waals-like bonding between the layers, which is not sensitive to the precise position of the atoms in each layer.

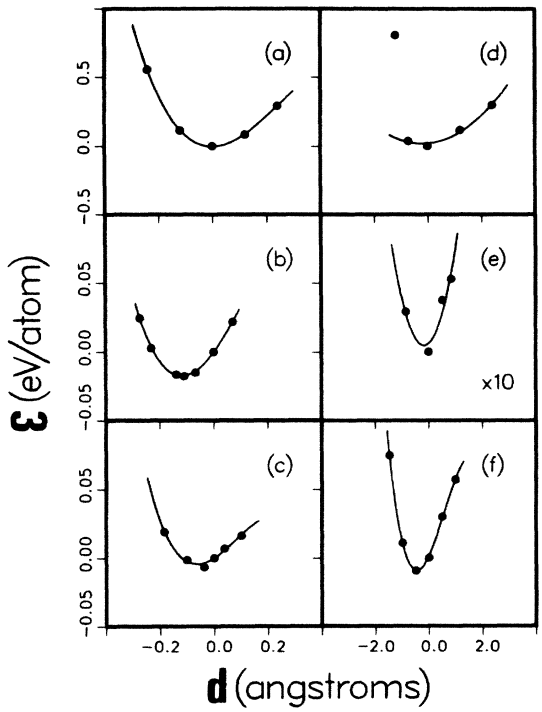

FIG. 4. Calculated total energy with respect to distortions of lattice parameters from experimentally measured values. (a) Uniform distortion in the bond lengths within layers keeping all other structural parameters fixed. (b) Intrachain bond-bending distortion. (c) Interchain bond-bending distortion. A unit of 0.2 Å is equivalent to an arc of 4.8°. (d) Rigid-layer shear along the a direction. (e) Rigid-layer shear along the c direction. (f) Variation in the lattice constant b keeping intralayer structural parameters fixed. Note difference in energy scales.

TABLE III. Computed force constants and phonon frequencies in the frozen phonon approximation. k_r is the bond-stretching force constant; $k_{\theta As}$ is the bond-angle-bending force constant with the bond-angle centered on As atoms; $k_{\theta Se}$ is the bond-angle-bending force constant with the bond-angle centered on Se atoms; k_a corresponds to shear along the a direction; k_b is the layer-compressional force constant; and, finally, k_c corresponds to shear along the c direction.

	Force constant	Phonon frequency (cm^{-1})
k_r	1.91×10^5 (dyn/cm bond)	
$k_{\theta As}$	$(5.2\pm0.2)\times10^4$ (dyn/cm angle)	
$k_{\theta Se}$	$(0.85\pm0.1)\times10^4$ (dyn/cm angle)	
k_a	1.3×10^3 (dyn/cm atom)	$\nu=34$
k_b	6.1×10^3 (dyn/cm atom)	$\nu=74$
k_c	0.16×10^3 (dyn/cm atom)	$\nu\sim12$

The total energies in Fig. 4 can also provide us with information concerning simple model force constants of the material. Moreover, if a particular distortion is close to an eigenmode we can obtain a direct measure of the phonon frequency associated with this mode. In fact, this should be the case for the interlayer distortions considered here. In Table III we present calculated intralayer and interlayer "bond" stretching and "bond" bending force constants. The phonon frequencies associated with the interlayer distortions are also included. The bond-stretching constant, k_r, agrees well with the value predicted using Gordy's rule[19] of 1.76×10^5 dyn/cm. The bond-bending constants are smaller than the bond-stretching constant by an order of magnitude. We find, furthermore, a large difference between the bond-bending constants of bonds centered at As and Se atoms, $k_{\theta As}$ being six times larger then $k_{\theta Se}$. This would seem to be consistent with the higher coordination number of the arsenic atoms implying a greater angular stiffness. These results are in rough agreement with simple force constant values derived empirically.[20]

The three rigid-layer *optical* phonon frequencies form a hierarchy with the compressional mode lying highest in frequency followed by the shear mode in the a direction (which destroys the fit of one "sawtooth pattern" upon another) and the second shear mode along the c direction (which retains the fit of one sawtooth pattern upon another). We find the phonon frequencies associated with the two rigid-layer shear modes to be ~12 and 34 cm^{-1} (see Table III). These shear modes have been identified by experiment as the two lowest Raman frequencies of the material[21] at 21.5 and 32.5 cm^{-1}. The comparison is very favorable for the higher mode frequency, while our accu-

racy is not adequate for the lower frequency with its associated small distortional energy. The third rigid-layer mode, the compressional mode, has been found to mix with intralayer bond-bending modes, and therefore not to be an exact eigenmode[21] (this can also be inferred from the similarly sized forced constants k_b and $k_{\theta Se}$ of Table III). The experimentally observed mode lies in the range 50—60 cm^{-1} which is not far from our 74 cm^{-1}.

Finally, let us consider the intralayer symmetry breaking energy in As_2Se_3. This can be estimated by imposing a reflection symmetry about the Se(3) atoms so that Se(1) and As(1) atoms have, respectively, identical intralayer environments to Se(2) and As(2) atoms. The resulting total-energy difference between the Vaipolin structure and the structure with the imposed intralayer reflection symmetry is roughly 2 meV per atom. It is interesting to note that two of the experimental determinations of the As_2Se_3 structure[7,9] differ mainly in the degree of bond-length variations. These variations are as much as 0.1 Å in the Vaipolin[7] structure but only 0.03 Å in the structure proposed by Kanisheva *et al.*[9] Thus the imposed intralayer reflection symmetry, just considered, roughly corresponds to transforming the Vaipolin[7] structure into the structure of Kanisheva *et al.*[9] The corresponding energy difference is extremely small and essentially outside the resolving power of our calculation.

C. Density of states

Before discussing details of the single-particle levels, let us first investigate the properties of the total density of states. This is shown in Fig. 5. The dashed line corresponds to an experimental photoemission measurement.[22] The solid lines are theoretical, one of which is broadened by 1 eV to simulate the resolution of experiment. Examination of the nonbroadened theoretical curve reveals four separate regions of nonzero density. As we shall see below, the two lowest regions correspond to the valence s levels. Of these, the lower one contains the 12 s levels of Se (since Se is more electronegative than As) and the higher one consists of the 8 s levels of As. The third region contains the valence p levels including 24 bonding and 12 lone-pair bands. The density of states in this region is consistent with earlier suggestions[5] that bonding and lone-pair states are not separated by a gap. The fourth region, separated from the third by the fundamental gap, corresponds to the empty 24 p-like antibonding levels. (Note that above these states there is another gap indicating a separation between the p antibonding levels and the $4d$-$5s$ states.)

The comparison with the experimental data is excellent. The peaks of the photoemission spectrum[22] line up with the theoretical density-of-states peaks, and the relative peak heights are also well reproduced. The latter is a

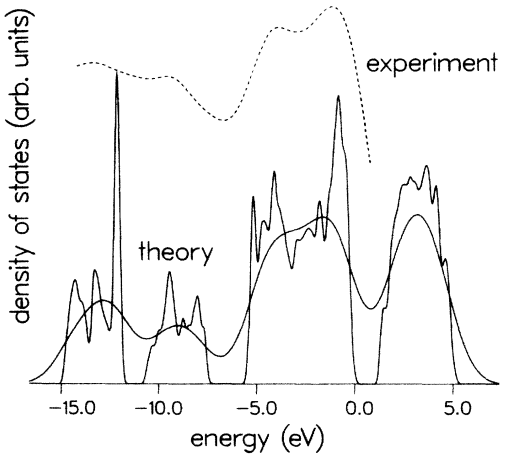

FIG. 5. Comparison of theoretical density of states (solid lines) with experimental photoemission measurements (Ref. 22) (dashed line). The smooth theoretical curve involves broadening by about 1 eV corresponding to the resolution of experiment. The top of the valence band is placed at 0 eV.

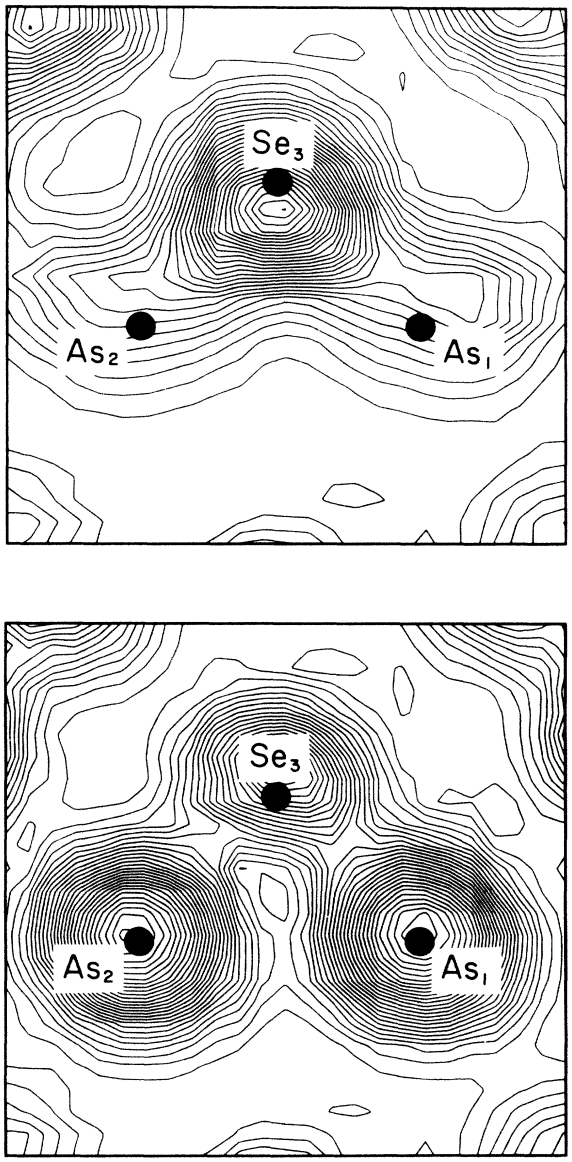

FIG. 6. Charge-density contours in plane III. Top panel, states in the region between −15 and −12 eV of Fig. 5. Bottom panel, states in the region between −11 and −7 eV.

consequence of the photoemission matrix elements being roughly equal for $4s$ and $4p$ valence electron scattering.

The charge densities of the three filled regions are presented sequentially in Figs. 6 and 7. Region one, corresponding to the upper panel in Fig. 6, shows a predominance of Se s-like character. Region two (lower panel) is much more antibonding s, with most of the charge localized around the As atoms. In Fig. 7 we show the charge density associated with region three. The upper panel corresponds to states in the energy range of about -5 to -2 eV. The plot is in plane III and illustrates the p-like bonding nature of these states. Finally, the lower panel corresponds to states in the energy range of -2 eV to the top of the valence band. The plot is in plane II and clearly reveals a p-like lone-pair character on the Se(1), Se(2), and Se(3) atoms.

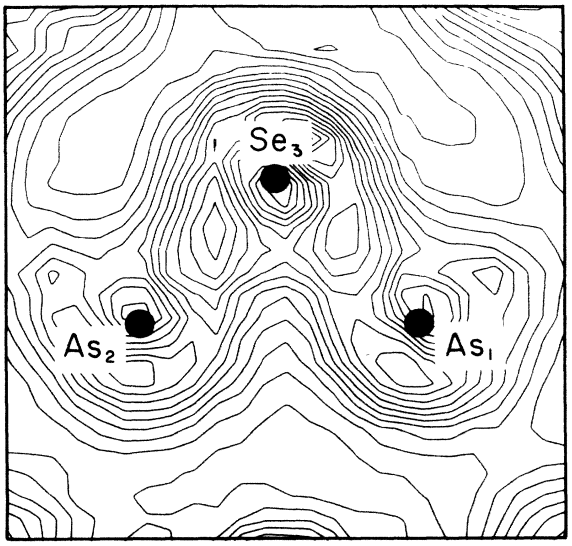

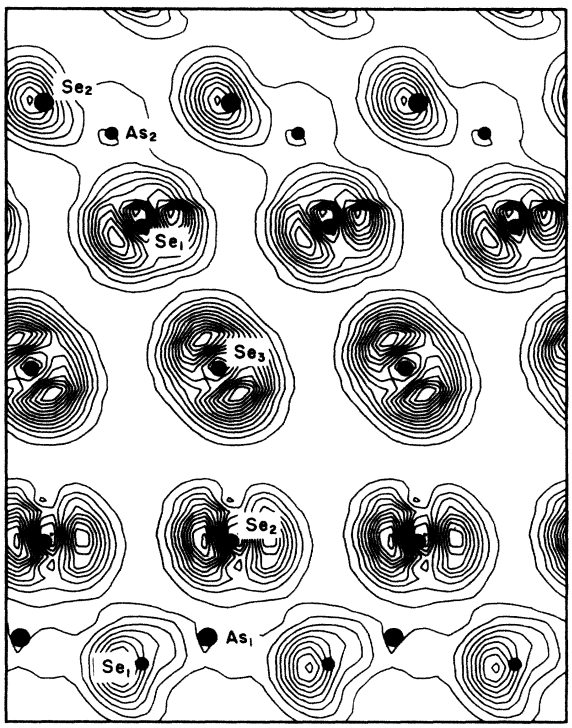

FIG. 7. Top panel, charge density in plane III for the region between -5 and -2 eV of Fig. 5. Bottom panel, charge density in plane II for the region between -2 eV and the top of the valence band.

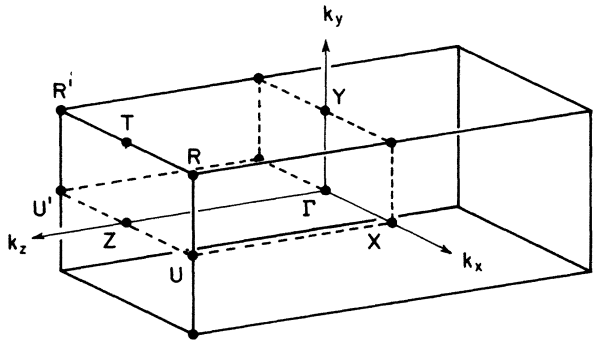

FIG. 8. Brillouin zone for the orthorhombic unit cell. The irreducible part is indicated by dashed lines. Several symmetry points are identified. For simplicity primes are used to distinguish inequivalent *directions* from Γ in the BZ.

D. Band structure

The Brillouin zone (BZ) for the orthorhombic cell is shown in Fig. 8. The band structure was calculated at 80 **k** points in eight directions of the irreducible part of this Brillouin zone. The results are depicted in Fig. 9. The large number of bands and the low symmetry of the crystal make the band structure quite complicated. Due to this complexity we will not discuss each band separately, but take a more perspective view.

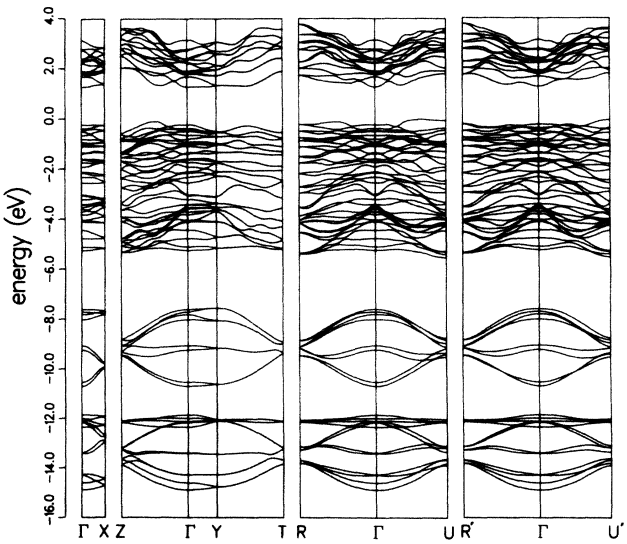

FIG. 9. Calculated band structure along specific directions in the Brillouin zone. Note the striking similarity between the $R-\Gamma-U$ and $R'-\Gamma-U'$ directions.

A detailed discussion of the symmetries and symmetry points of the Brillouin zone has been given by Althaus *et al.*[5] The bands are doubly degenerate on the Y-T line due to time-reversal symmetry. Further degeneracies occur at the X, Y, and Z points where the bands are described by two-dimensional symmetry-group irreducible representations.[5]

The Se lone-pair states and the p-bonding states seem to overlap everywhere in **k** space, except possibly in the region of -1.5 eV on the symmetry line between Y and T. Nevertheless, this overlap is small and the top 12 valence bands consist of almost pure lone-pair states as we have already seen in Fig. 7 (bottom panel).

The widths of the p-like bonding bands and the lone-pair bands remain nearly constant from one **k** point to the next throughout the entire BZ. This is a consequence of the high degree of localization of these bands. While the 4 nonbonding Se s levels also remain relatively unbroadened, the 16 bonding As and Se s levels enjoy a considerable dispersion, being very wide at Γ and becoming narrow as we approach the BZ edges. The dispersions of the bands along the layer stacking direction as opposed to within a layer, tend to be fairly flat. This is clear, for example, by comparing the direction $\Gamma-Y$ with $\Gamma-Z$ and $\Gamma-X$ in Fig. 9. Upon close examination, however, we note that the p-like bonding states seem to have very similar dispersion both between and within the layers. No doubt this is related to the interlayer overlap of these wave functions as we discussed earlier.

Let us now examine to what extent the *intralayer* symmetry breaking effects differences in the band structure. The symmetry operator that is broken is a reflection in the b-c plane, passing through Se(3) atoms. If this symmetry existed, As(1) and Se(1) atoms would be identical within the intralayer environment to As(2) and Se(2) atoms, respectively. If, in addition, the layers were stacked so that the Se(3) atoms all lay in a plane the bands along $R-\Gamma-U$ would be identical to those along $R'-\Gamma-U'$. We note from Fig. 9, that this, indeed, is very nearly the case. The largest differences appear to be on the order of a few tenths of an eV and occur primarily in the vicinity of the fundamental gap.

It is interesting to investigate the effects of the layer-layer interactions on the total widths of the energy bands. To accomplish this we moved the layers far apart (a disance of 10 Å) and examined the single-particle levels at Γ. (Unfortunately, the large size of the unit cell made any attempt at a full band structure intractable.) In the presence of layer-layer interactions the widths of the bands (see Fig. 9) are as follows: 3 eV for the Se s states, 3 eV for the As s states, and 5 eV for the p-bonding and lone-pair states. The corresponding widths of *separated* layers are smaller by 0.4, 0.2, and 0.7 eV, respectively. Furthermore, the "gap" at Γ between lone-pair and p-bonding states increased from 0.2 to 0.4 eV. These results imply that the layer-layer interactions are responsible for a small overall broadening of each band region by ~ 0.5 eV.

Experimentally, it has not yet been determined precisely where in the BZ the fundamental gap obtains. It is believed that the bottom of the conduction band is at Γ[5]. Nothing, however, is known about the position of the top of the valence band. Using the results of the band structure in Fig. 9, as well as a systematic search over 108 **k** points within the irreducible BZ, we were able to identify several candidates. These are extrema that lie within 0.1 eV of each other, which corresponds to the extent to which systematic errors may enter. The results are summarized in Table IV. There are five lowest minima of the conduction band that lie within the range of 0.1 eV, but only one maximum of the valence band. The top of the valence band lies very nearly along the $\Gamma-U$ direction. In fact, this is directly related to what appears to be a maximum roughly midway between Γ and U in Fig. 9. From Table IV the fundamental gap is clearly indirect and most likely associated with either (0.23,0.31,−0.12) or Γ. The five indirect gaps, however, lie very close in energy ranging from 1.26 to 1.36 eV. We find three candidates for the smallest *direct* gap. These are also presented in Table IV. We note that one of the direct gaps is at Γ which is consistent with recent experimental observations.[23] The other two direct gaps, which are at nonsymmetry points, lie very close in energy. Finally, we note that our results predict at least five indirect transitions before the onset of direct transitions. This is also consistent with the experimental result of "at least three."[24]

Effective masses were calculated at the top of the

TABLE IV. Band-edge extrema and direct gaps within a tolerance of 0.1 eV, as discussed in the text.

	Energy (eV)
Valence maximum:	
(0.29,0,0.31)	0
Conduction-band minima:	
(0.23,0.32,−0.12)	1.26
(0,0,0)	1.29
(1/12,5/12,5/24)	1.33
(5/12,3/12,3/24)	1.35
(1/12,1/12,5/24)	1.36
Direct gap:	
(1/12,1/12,5/24)	1.47
(0,0,0)	1.50
(1/12,3/12,−5/24)	1.56

TABLE V. Hole and electron effective masses with corresponding principal axes. The principal axes are given in terms of crystal-axis unit vectors $\hat{a},\hat{b},\hat{c}$.

	m^*/m_e	Principal axes
Hole	0.28	(0.86,0,−0.51)
±(0.29,0,0.31)	1.0	(0.51,0,0.86)
	1.1	(0,1,0)
Electron	2.8±0.6	(0.45,−0.44,0.78)
(0.23,0.31,−0.12)	1.2	(−0.67,0.41,0.62)
	0.33	(0.59,0.80,0.11)
(0,0,0)	0.27	(0.38,0,0.92)
	1.6	(0.92,0,−0.38)
	5.7	(0,1,0)

valence band and at the two lowest minima of the conduction band. The results are presented in Table V. From symmetry, the electron (Γ) and hole masses are restricted to have one of their principal axes normal to the layers. The hole at the top of the valence band can exist at two possible **k** points in the BZ. These are related by inversion symmetry and the hole masses have the same principal axes. We note that the hole has a mass that is nearly isotropic in a plane perpendicular to the layers with $m^* \sim m_e$. This is much smaller than expected. Intuitively both the holes and the electrons should have heavy masses perpendicular to the layers. Moreover the hole mass should be greater. However, there is only one heavy mass perpendicular to the layers, and it belongs to the *electron*. Notable also, is the large anisotropy in the electron masses, particularly at Γ. The very light electron (Γ) and hole mass components lie in a plane parallel to the layers and run along directions that are nearly orthogonal to each other. On the other hand, the light electron mass component at (0.23,0.31,−0.12) has a sizable projection *perpendicular* to the layers. Unfortunately, at this time we have no simple physical picture as to why these particular eigendirections are chosen.

E. Nature of states at band edges

Let us now investigate the properties of the states lying in the vicinity of the band edges of the fundamental gap.

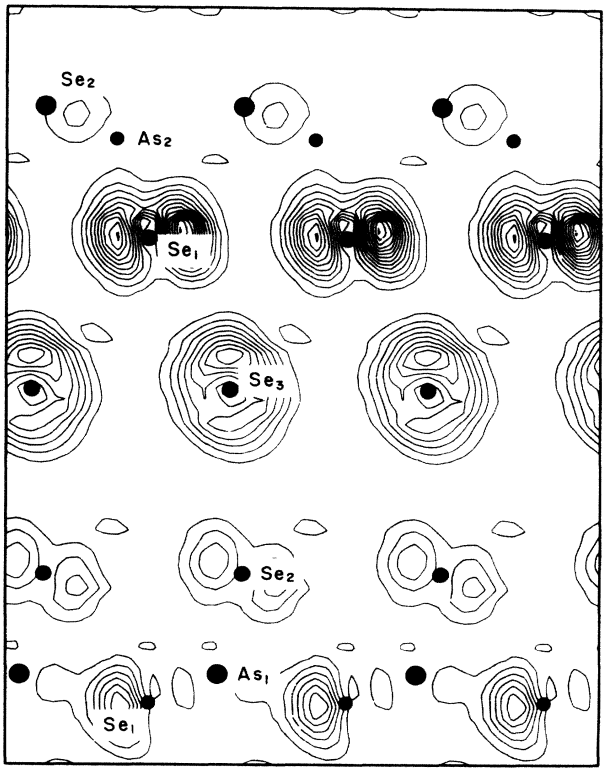

FIG. 10. Charge density of uppermost filled valence band in plane II. Note the absence of charge on Se(2).

We are specifically interested in the atomic character, orbital character, and localized nature of these states and their sensitivity to interlayer interactions. To do this we shall examine the charge densities associated with the uppermost filled valence band and the lowest empty conduction band. We begin our analysis with the valence band.

To examine the charge density near the top of the valence band it is convenient to use plane II. We recall that in Fig. 7 (bottom panel), plane II clearly reveals the Se(1), Se(2), and Se(3) p-like lone-pair character of the states lying between −2.0 and 0 eV. The corresponding charge density for the uppermost filled valence band is shown in Fig. 10. We find a very interesting result. Unlike Fig. 7 (bottom panel), most of the charge is on Se(1), there is some charge on Se(3) and hardly any on Se(2)! How can we understand this? As it turns out, it can be explained as a direct consequence of the interaction between Se atoms in different layers. A close examination of the arrangement of the Se atoms in Fig. 1 reveals that Se(1) and Se(3) atoms on neighboring layers interact much more strongly with each other than with Se(2) atoms. This strong interaction creates the lone-pair states which lie furthest away from the center of the lone-pair band. At the top of the valence band, it leads to antibonding lone-pair states with charge primarily localized on Se(1) and Se(3) atoms.

If this analysis is correct, one should not expect to observe this behavior if the layers were isolated from each other. To simulate this isolation, we consider again our model crystal containing layers separated by 10 Å. The charge density of the uppermost filled valence band is shown in the left panel in Fig. 11. We now find a very different result! This is p-like lone-pair charge on Se(1) and Se(2) atoms but hardly any charge on Se(3). To make sure that this is not an artifact of the slight change in plane, we include, in the right panel of Fig. 11, the charge density of the entire lone-pair region between −2.0 and 0 eV. The localized p-like character is clearly evident on the Se(1), Se(2), and Se(3) atoms.

This result can be understood as follows. Once the layers are so far apart, the only important interactions are between Se atoms within a layer. From Fig. 1 we notice that the Se(3) atoms are fairly well isolated from an *intra*layer point of view. Thus the strongest interactions are between the Se(1) and Se(2) atoms which are members of the spiralling chains. This interaction then leads to states at the top of the valence band being antibonding combinations of lone-pair orbitals localized primarily on Se(1) and Se(2) atoms.

To investigate the nature of the empty states in the conduction band it is convenient to examine charge densities in plane III. This is the plane that contains Se(3) and, its two nearest neighbors, As(1) and As(2). One would expect the first 24 empty energy bands to correspond to p-like antibonding states. The states that lie lowest in energy are very symmetrical and tend to place charge in the region *between* neighboring As—Se bonds. This is illustrated in the top panel of Fig. 12. Here we display the charge density associated with the lowest empty conduction band. The charge near the Se(3) atoms is associated with the neighboring pairs Se(3)-As(1) and Se(3)-As(2). Similarly

the charge near each As atom is associated with the three bonds each As atom makes with its neighboring Se atoms, two of which lie above and below the plane. We note that most of the charge is localized near the As atoms. This is consistent with the simple view that antibonding states should be more cationlike. This is not always true, however, and in GaAs, for example,[25,26] the lowest conduction band is anionlike. This is because the larger disparity be-

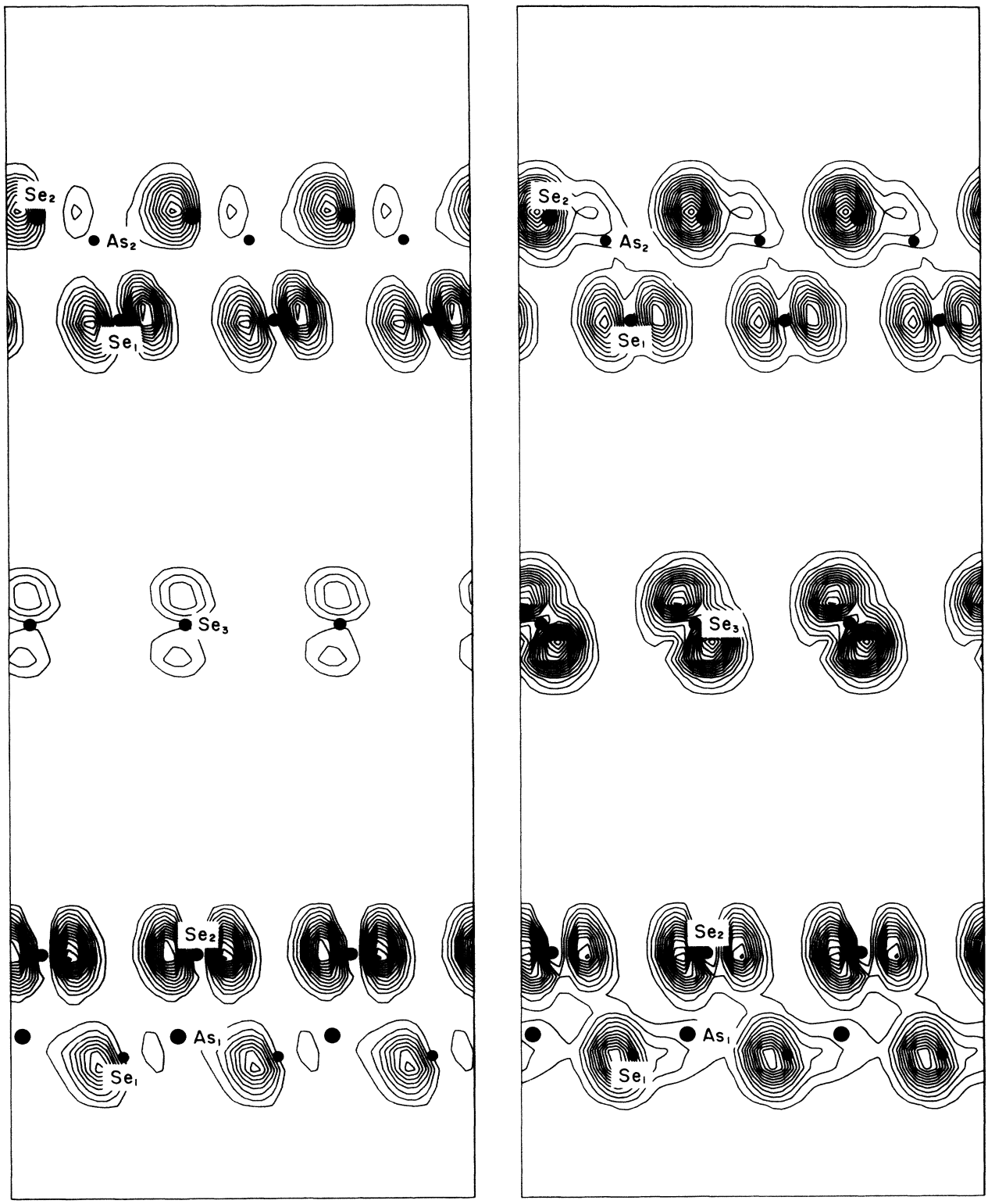

FIG. 11. Charge density for a model crystal with layers separated by 10 Å in plane II'. Left panel, uppermost filled valence band. Right panel, the entire lone-pair region.

tween the Ga and As potentials which allows excited anion states to lie comparatively low in energy. For As and Se, the potentials are fairly similar and this does not occur.

In the bottom panel of Fig. 12 we show the effects of moving the layers far apart. Although we now find less charge near Se(3), the overall charge density is very similar. These states, therefore, do not appear to be very sensitive to the interlayer interactions.

Finally, using these results we can speculate as to the effects of disorder on the fundamental gap in the glass. Even if the atoms are perfectly and stoichiometrically bonded, variations in the intralayer topology would cause variations in the interlayer environment. From the discussion above we expect this to create a fair amount of dispersion and localization of states near the top of the valence band. The bottom of the conduction band would be affected less by this specific type of disorder. This would imply that the conduction-band mobility should be larger than the valence-band mobility. This, however, is contrary to what is observed experimentally.[27] Only holes are found to be mobile in very pure glassy samples. Of course, in our discussion we have neglected the effects of intrinsic defects which could play an important role in trapping electrons. The precise mechanism for this, however, is not presently understood.

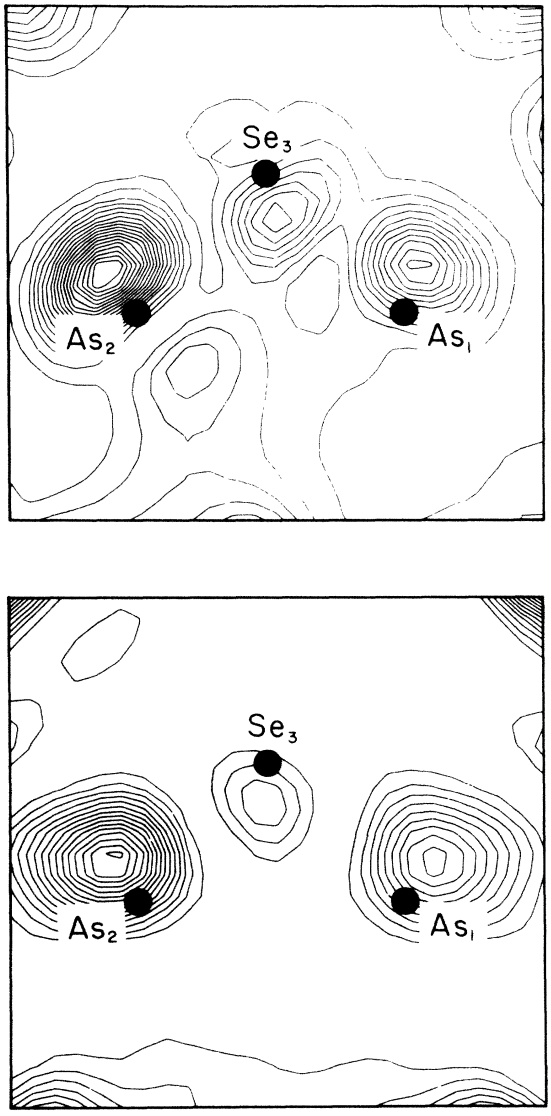

FIG. 12. Charge densities in plane III associated with the lowest conduction band. Top panel, the normal crystal. Bottom panel, the crystal with interlayer separation increased to 10 Å.

F. Cohesive and bonding energies

The cohesive energy of the solid ($E_{\rm coh}$) can be calculated by comparing the total energy of the solid at equilibrium with the total energy of an equivalent number of isolated atoms at infinity. In our case these would be isolated pseudoatoms including their spin-polarization energy. We obtain a value of 3.3 eV per atom or roughly 2.7 eV per bond. An experimental measurement of the cohesive energy has not been performed. The cohesive energy, however, can be estimated using the measured heat of fusion ($E_{\rm hof}$) of the compound from elemental solids[28] and the measured enthalpy of formation ($E_{\rm eof}$) of the elemental solids.[29] Thus if we have

$$\mathrm{As_2Se_3(solid)} \Longrightarrow 2\,\mathrm{As(solid)} + 3\,\mathrm{Se(solid)} - E_{\rm hof} ,$$

$$\mathrm{As(solid)} \Longrightarrow \mathrm{As(gas)} - E_{\rm eof,As} ,$$

$$\mathrm{Se(solid)} \Longrightarrow \mathrm{Se(gas)} - E_{\rm eof,Se} ,$$

then

$$E_{\rm coh} = 2E_{\rm eof,As} + 3E_{\rm eof,Se} + E_{\rm hof} .$$

Experimentally we have $E_{\rm eof,As} = 72.04$ kcal/mole, $E_{\rm eof,Se} = 54.1$ kcal/mole, and $E_{\rm hof} = 9.75$ kcal/mole so that $E_{\rm coh} = 316$ kcal/mole $= 13.7$ eV/$\mathrm{As_2Se_3}$ molecule $= 2.7$ eV/atom $= 2.3$ eV/bond.

The difference between this value and our theoretical prediction is about 20%. As we have mentioned earlier, this is very good considering that it involves differences in energy between substantially different systems, i.e., isolated atoms and the bulk solid.

From our calculations we can also obtain a reasonable estimate of the contribution to the cohesive energy from the binding *between* layers. This is not known experimentally but can be deduced, theoretically, by dissecting the solid into isolated layers at infinity. To do this we again use our results from the model crystal containing layers separated by 10 Å. We obtain a value of about 0.3 eV per atom for the binding energy between layers. This is about 10% of the total cohesive energy and is larger than typical van der Waals energies which are about 0.01—0.1 eV. This is also consistent with the fact that the layers are about 20% closer than their typical van der Waals distance.

These results can be analyzed using the following heuristic argument. The van der Waals interaction can be considered as a second-order correction to the total energy of the form

$$E_{\rm van\,der\,Waals} = -\,|H|^2/\Delta E .$$

Here H represents a matrix element that involves transi-

TABLE VI. Tight-binding fit to band structure of Fig. 9 including nearest-neighbor interactions within a single layer. The resulting band structure is shown in Fig. 14.

$E_{s,As}=-7.9$ eV	$E_{s,Se}=-10.8$ eV	$E_{p,As}=2.6$ eV	$E_{p,Se}=0$
$V_{pp\pi}=-1.8$ eV	$V_{pp\sigma}=2.4$ eV	$V_{ss}=-1.5$ eV	
$V_{s,As,p,Se}=-2.0$ eV	$V_{p,As,s,Se}=0$ eV		

tions from the unperturbed ground state of each layer to all possible excited states of the layers. Included, therefore, are exchange transitions from one layer to a neighboring layer. Usually these terms are ignored because the typical overlap between molecules is extremely small. One might be tempted to argue, however, that in As_2Se_3 this overlap may not be so negligible. After all, we have already seen from Fig. 2(a) that there is at least some charge between the layers in the ground state. Moreover, this is also true for the excited states as shown in Fig. 13. Here we have plotted the charge density, for the lowest 24 empty conduction bands, in plane I. We note again a non-negligible amount of charge between the layers. Even so, the contribution from intralayer polarization should be much larger and completely dominate the exchange terms. Another possibility is that ΔE is small. This is more attractive since the average optical gap for As_2Se_3 is only about 3.5 eV. This is in contrast to the much larger energy gaps that one would expect for atoms and molecules. Finally, since the van der Waals interaction in As_2Se_3 is between *layers*, the $|H|^2$ term should go like $1/R^4$ instead of $1/R^6$. This would have the tendency to make the van der Waals equilibrium distance shorter.

G. Tight-binding fit

When one is interested in describing the electronic structure of complex systems such as defects in solids, or even glassy solids, realistic theoretical approaches are usually intractable. It is often necessary, therefore, to formulate a much simpler theoretical model. A very useful technique involves modeling the valence electrons in terms of a simple empirical tight-binding Hamiltonian. The matrix elements of this Hamiltonian are usually fit to the crystal band structure of a realistic calculation. Since the results of this work represent the first such band structure, it would seem appropriate to include a brief analysis in terms of simple tight-binding theory. We will use a model with the least number of adjustable parameters. Our purpose is to see how much of the realistic band structure will be preserved, and thus can be thought of in very simple terms.

Our model is appropriate for a simple isolated layer. The charge-density calculations indicate that the filled valence band and lowest empty conduction states can be adequately described with basis functions consisting of only one s-like orbital and three p-like orbitals per atom. The orbitals are taken to be mutually orthogonal and only nearest-neighbor interaction matrix elements are assumed nonzero. In addition, bond-length variations are taken into account using a $(d_0/d)^2$ dependence with $d_0=2.4$ Å. The parameters resulting from our fit are given in Table VI. $V_{p,As,s,Se}$ was found to have little influence on the band dispersions and was set to zero for simplicity. The

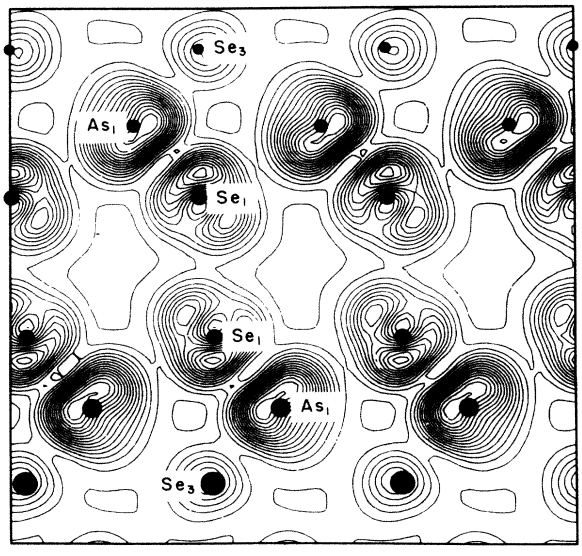

FIG. 13. Charge density associated with the lowest 24 conduction bands in plane I.

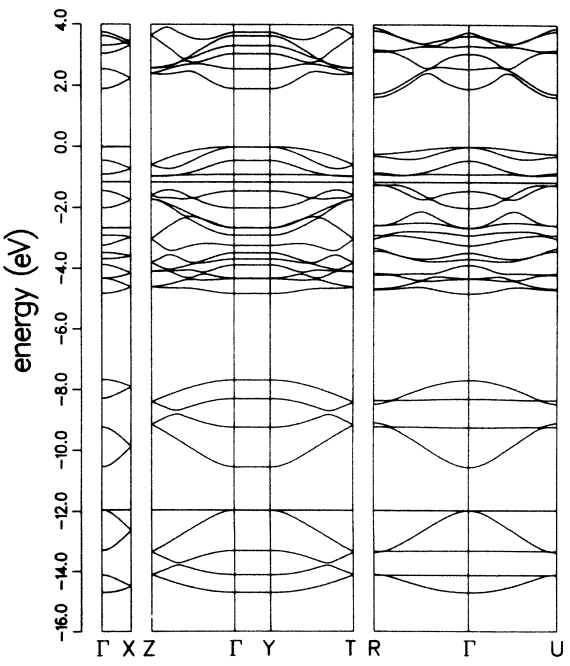

FIG. 14. Tight-binding band structure for an isolated As_2Se_3 layer. The redundant symmetry points R, T, and Y are included for ease of comparison with Fig. 9. The tight-binding parameters are given in Table VI.

corresponding band structure using these parameters is shown in Fig. 14. We note that the dispersion of the Se and As s-like bands are reproduced fairly well. Moreover, several gross features of the realistic p bands can be identified. The conduction band, however, is less well described. Clearly, the inclusion of second-neighbor interactions would bring about much better agreement. This would lead to interactions between the layers and introduce dispersion along the Y direction. Moreover, it would create dispersion of the flat nonbonding s levels and cause splitting of bands throughout most of the BZ.

V. SUMMARY

Our results, derived from first principles using only the atomic numbers of As and Se, are in excellent agreement with experiment wherever comparisons have been possible. Firstly, the equilibrium bond length is correct to within 1% of the experimental value, the equilibrium angles are correct to within 3% and the equilibrium interlayer distance and the layer-layer positions are correct to within 5%. Secondly, the averaged density of states agrees very well with an experimental photoemission spectrum. Thirdly, the position of the direct gap in the BZ and the number of indirect transitions before the onset of direct transitions are consistent with experimental findings.

Furthermore, quantitative *predictions* for experimental results have been possible. The positions of the band-edge extrema have been determined, and the lowest-lying indirect and direct gaps identified. It is predicted that the effective-mass spectrum should show an unusually rich behavior including a large anisotropy in magnitude of the electron masses and a light hole *perpendicular* to the plane of the layers. In addition, the hole band mobility should be much more sensitive to fluctuations in interlayer separation than the mobility of the electron.

We found conceptually simple models of the electronic states to be valid. Thus the valence band and the lowest conduction bands can be adequately described in terms of s and p orbitals and their bonding, antibonding, and nonbonding configurations. For example, Se lone-pair states can be identified, they are indeed nonbonding p like, and do not mix substantially with the p-like bonding states. This occurs even though the two types of states are not separated by an energy gap.

The material displays several different energy scales associated with structural distortions. Bond-length force constants are much larger than bond-bending force constants, and the bond angles centered around the As atoms are stiffer than bond angles centered on the Se atoms. The three interlayer optical-phonon modes form a hierarchy with the compressional mode lying the highest in frequency and the shear mode along the c direction the lowest.

Finally, the cohesive energy an be split up into intralayer and interlayer contributions, with a corresponding ratio of about 10:1. The interlayer van der Waals interaction is thus unusually strong, which may be interpreted as arising from the layerlike structure and small optical gap of the material.

ACKNOWLEDGMENTS

This work was supported in part by a National Science Foundation Grant, No. DMR-84-18718. One of the authors (A.A.) would like to thank the Brazilian Fundaçao de Amparo a Pesquisa do Estado de São Paulo (FAPESP) and Conselho Nacional de Desenvolvimento Científico e Technólogico (CNPq) for financial support.

[1]N. F. Mott and E. A. Davis, *Electronic Processes in Non-Crystalline Materials* (Clarendon Press, Oxford, 1979).

[2]For recent progress, see, for instance, Proceedings of the Eleventh International Conference on Amorphous and Liquid Semiconductors [J. Non-Cryst. Solids **77&78**, 1 (1985)].

[3]A. I. Gubanov and S. M. Dunaevskii, Fiz. Tekh. Poluprovodn. **8**, 716 (1974) [Sov. Phys.—Semicond. **8**, 457 (1974)].

[4]S. G. Bishop and N. J. Shevchik, Phys. Rev. B **12**, 1567 (1975).

[5]H. L. Althaus, G. Weiser, and S. Nagel, Phys. Status Solidi **87**, 117 (1978).

[6]D. W. Bullett, Phys. Rev. B **14**, 1683 (1976).

[7]A. A. Vaipolin, Sov. Phys. Crystallogr. **10**, 509 (1966).

[8]A. L. Renninger and B. L. Averbach, Acta Crystallogr. B **29**, 1583 (1973).

[9]A. S. Kanisheva, Yu. N. Mikhailov, E. G. Zhukov, and T. G. Grevtseva, Izv. Akad. Nauk SSSR, Neorg. Mater. [Inorg. Mater. (USSR) **19**, 1981 (1983)].

[10]J. D. Joannopoulos, *Physics of Disordered Materials*, edited by D. Adler, H. Fritsche, and S. R. Ovshinsky (Plenum, New York, 1985), and references therein.

[11]E. P. Wigner, Phys. Rev. **46**, 1002 (1934).

[12]D. R. Hamann, M. Schlüter, and C. Chiang, Phys. Rev. Lett. **43**, 1494 (1979).

[13]A. Baldereschi, Phys. Rev. B **7**, 5212 (1973); D. J. Chadi and M. L. Cohen, *ibid.* **8**, 5747 (1973).

[14]All reciprocal coordinates will be given in terms of reciprocal lattice vectors $(2\pi/a,0,0)$, $(0,2\pi/b,0)$, and $(0,0,2\pi/c)$.

[15]P.-O. Löwdin, J. Chem. Phys. **19**, 1396 (1951).

[16]K. Ho, J. Ihm, and J. D. Joannopoulos, Phys. Rev. B **25**, 4260 (1982).

[17]M. Schlüter, Int. J. Quantum Chem. **7**, 527 (1973).

[18]D. Vanderbilt and J. D. Joannopoulos, Phys. Rev. B **27**, 6296 (1983).

[19]W. Gordy, J. Chem. Phys. **14**, 305 (1946).

[20]G. Lucovsky, Phys. Rev. B **6**, 1480 (1972); G. Lucovsky and F. L. Galeener, J. Non-Cryst. Solids **37**, 53 (1980).

[21]R. Zallen and M. Slade, Phys. Rev. B **9**, 1627 (1974).

[22]See, R. Zallen and D. F. Blossey, *Optical and Electrical Properties of Compounds with Layered Structure*, edited by P. A. Lee (Reidel, Dordrecht, 1976), p. 231.

[23]H. L. Althaus and G. Weiser, Phys. Status Solidi B **99**, 537 (1980).

[24]H. L. Althaus and G. Weiser, Phys. Status Solidi B **99**, 277 (1980).

[25]Eugene J. Mele and J. D. Joannopoulos, Surf. Sci. **66**, 38 (1977).
[26]Y. Wang and J. D. Joannopoulos, J. Vac. Sci. Technol. **17**, 997 (1980).
[27]See, for instance, M. E. Scharfe, Phys. Rev. B **2**, 5025 (1970).
[28]M. B. Myers and E. J. Felty, J. Electrochem. Soc. **117**, 818 (1970).
[29]R. Hultgren, P. D. Desai, D. T. Hawkins, M. Gleiser, K. K. Kelley, and D. D. Wagman, *Selected Values of the Thermodynamical Properties of the Elements* (American Society of Metals, Cleveland, 1973).